Published in final edited form as:
J Neurochem. 2011 August ; 118(4): 499–511. doi:10.1111/j.1471-4159.2011.07274.x.

Small molecule analysis and imaging of fatty acids in the zebra finch song system using time-of-flight-secondary ion mass spectrometry

Kensey R. Amaya[a,c], **Jonathan V. Sweedler**[b], and **David F. Clayton**[a]

[a] Department of Cell and Developmental Biology, University of Illinois at Urbana-Champaign, 601 S. Goodwin Ave., Urbana, IL 61801; Ph: 217-244-3668; fax: 217-244-1781

[b] Department of Chemistry, University of Illinois at Urbana-Champaign, 600 S. Mathews Ave., Urbana, IL 61801; Ph: 217-244-7359; fax: 217-244-8068

Abstract

Fatty acids are central to brain metabolism and signaling, but their distributions within complex brain circuits have been difficult to study. Here we applied an emerging technique, time-of-flight secondary ion mass spectrometry (ToF-SIMS), to image specific fatty acids in a favorable model system for chemical analyses of brain circuits, the zebra finch (*Taeniopygia guttata*). The zebra finch, a songbird, produces complex learned vocalizations under the control of an interconnected set of discrete, dedicated brain nuclei “song nuclei”. Using ToF-SIMS, the major song nuclei were visualized by virtue of differences in their content of essential and non-essential fatty acids. Essential fatty acids (arachidonic acid and docosahexaenoic acid) showed distinctive distributions across the song nuclei, and the 18-carbon fatty acids stearate and oleate discriminated the different core and shell subregions of song nucleus LMAN. Principle component analysis of the spectral data set provided further evidence of chemical distinctions between the song nuclei. By analyzing song nucleus RA at three different ages during juvenile song learning, we obtain the first direct evidence of changes in lipid content that correlate with progression of song learning. The results demonstrate the value of ToF-SIMS to study lipids in a favorable model system for probing the function of lipids in brain organization, development and function.

Keywords

SIMS; imaging; arachidonic acid; docosahexaenoic acid; brain; songbird

Introduction

Fatty acids comprise a diverse group of unbranched carboxylic acids, with variable numbers of carbon chains and degrees of saturation. They are central in cell metabolism and also form a primary structural component of all cell membranes (as phospholipids). They also have major roles in cell signaling – and nowhere more so than in the brain. Membrane phospholipids are precursors for the generation of numerous messenger compounds active in the brain including prostaglandins and platelet-activating factor (Bazan, 2005), endocannabinoids (Piomelli, 2005), and diacylglycerol (Kim et al., 2010). Local variations

To whom correspondence should be addressed: Dr. David F. Clayton; dclayton@illinois.edu.
[c]current address: U.S. Army Engineer Research and Development Center, Construction Engineering Research Laboratory (ERDC-CERL), P.O. Box 9005 Champaign, IL 61821; Ph: 217-352-6511 x7551; fax: 217-373-7222

Authors report no conflict of interest.

in specific lipid content contribute to the structure of synaptic junctions (Suzuki, 2002), and growing evidence suggests that specific synaptic lipids regulate vesicle exocytosis and membrane recycling (Davletov & Montecucco, 2010). Of particular interest are the essential fatty acids (EFAs) – polyunsaturated fatty acids that are derived from the diet and important in in cognitive function (Moriguchi *et al.* 2000), inflammatory and immunological responses (Simopoulos, 2002; Bazan, 2005), and brain development (Innis, 2008). Polyunsaturated fatty acids (PUFAs) are notably vulnerable to oxidative damage (and conversely, may also participate in protection against oxidative damage) and have been implicated as promoting or protective factors in a range of neurological diseases, including Alzheimer's (Hartmann *et al.* 2007), Parkinson's (Israeli & Sharon 2009) schizophrenia (Fenton *et al.* 2000) and epilepsy (Cole-Edwards & Bazan 2005).

A better understanding of the diversity of fatty acids and their specific local distributions and functions will therefore be critical for a broad range of issues in neurobiology. However, the tools for studying fatty acid distributions in brain have been limited compared to the tools available for analysis of proteins and nucleic acids. Studies have typically relied on dissection, homogenization, and detection – methods that do not provide information about cellular or subcellular distributions. Specific lipids can be visualized with fluorophore labels but this is limited to cases where labeled lipids can be applied exogenously, and these labels can adversely affect lipid-lipid and lipid-protein interactions (Maier *et al.* 2002).

Time-of-flight secondary ion mass spectrometry (ToF-SIMS) is an alternative approach that allows direct surface visualization of intrinsic, unlabeled small molecules (<1,000 *m/z*) in tissue sections at a lateral resolution of ~1 μm (Ewing 2006, Johansson 2006, Mas *et al.* 2008). The technology has been shown to be a robust tool for the detection and imaging of lipids in a diverse array of tissues such as muscle (Tahallah *et al.* 2008), nervous system (Pernber *et al.* 2007), and kidney (Nygren *et al.* 2004). Subcellular imaging with ToF-SIMS has also revealed significant localization of other lipophilic molecules such as vitamin E in isolated neurons from *Aplysia californica* (Monroe *et al.* 2005) and has been used in several studies on the mammalian spine (Monroe, *et al.* 2005, Monroe *et al.* 2008).

In this report, we describe the application of ToF-SIMS to develop a primary analysis of the distribution of fatty acids within the brain of both adult and developing zebra finches. The zebra finch (*Taeniopygia guttata*), a songbird, is an important model for neuronal circuitry development, neurogenesis, learning and memory, and its genome was recently sequenced (Warren *et al.* 2010). A distinctive feature of the songbird brain, which makes it especially conducive to focal molecular analysis, is the presence of several large anatomical nuclei in the forebrain that are interconnected in a circuit (Fig. 1) that controls the learning and production of birdsong (reviewed in (Brenowitz *et al.* 1997, Clayton *et al.* 2009, Zeigler & Marler 2004). These nuclei have been studied intensively for their physiological and developmental properties (Clayton 1997) and they form a valuable reference set for studies of molecular composition in the brain (Lovell *et al.* 2008). In the zebra finch, this “song control circuit” is completed during a critical period in juvenile development (between about 20 and 40 days post-hatch), and only in males (females do not produce learned vocalizations). It is during this critical period that a young male zebra finch learns to sing by copying the song of an adult tutor. With sexual maturity, the ability to further modify the song or learn a new one is essentially lost.

Several observations suggest important roles for lipids and fatty acids in song system development and function. One of the first genes shown to be developmentally regulated within the song control circuit encodes the ortholog of alpha-synuclein (originally referred to as synelfin, (George *et al.* 1995)), a lipid-binding protein subsequently implicated in Parkinson's and other neurodegenerative diseases (Clayton & George 1999). Lipophilic

molecules, including retinoic acid (Jeong *et al.* 2005, Denisenko-Nehrbass *et al.* 2000), cannabinoids (Soderstrom et al., 2004) and sex steroids (London *et al.* 2006), are synthesized in or near several of the song control nuclei and are necessary for song learning and song circuit development. Yet the lipid and fatty acid composition of the zebra finch brain has remained largely unexplored. Indeed, information about brain lipids is sparse for all birds in comparison to mammals, and mostly limited to issues related to embryogenesis, metabolic rate and egg production (e.g., (Maldjian et al., 1996; Speake & Wood, 2005; Turner, 2005).

We previously used ToF-SIMS to image the distributions of several inorganic ions and lipids in the songbird brain (Amaya *et al.* 2007). Here we analyze the distribution of fatty acids and other lipids across the major forebrain components of the song system, both in adults and during the critical period for song learning and circuit development. In order to facilitate analysis of the complex datasets, we incorporate principle component analysis (PCA) into our measurements to determine regional and age-related differences in content. Our results reveal a complex distribution of fatty acids across different song nuclei, and set the foundation for future targeted studies to address the potential functional importance of these fatty acids in this important model of neural circuit development and function.

Materials and Methods

Tissue preparation and staining

All animal procedures were conducted according to protocols approved by the University of Illinois Institutional Animal Care and Use Committee. Male zebra finches were sacrificed by rapid decapitation, the brain removed, and rapidly frozen on dry ice. Post-hatch day 20 birds were sexed postmortem by gonadal identification. Parasagittal sections, 16 μm in thickness, were collected beginning at 2.5 mm to the midline (~5.6 mm) and alternatively placed on either a glass slide for histological staining, or a glass cover slip for ToF-SIMS and immunohistochemical analyses. Sections were stored at –80 °C for no more than 3 wks. Histological staining by cresyl violet was carried out as previously described (Amaya et al. 2007). Sections were identified that contained the major components of the forebrain song system: nucleus RA, nucleus HVC (used as a proper name), lateral magnocellular nucleus of the nidopallium (LMAN), dorsolateral thalamic nucleus (DLM), AreaX, and the NCM/CMM complex comprising the AL (Fig. 1). The adjacent sections then used for ToF-SIMS or immunohistochemical analysis.

ToF-SIMS and image analysis

Sections from adult males (n=3) were removed from –80 °C storage and immediately vacuum dried (~15 min) at room temperature. Dried sections were placed in a Desk II TFC sputter coater (Denton Vacuum, Moorestown, NJ) equipped with a gold target and ~10 Å was deposited on sample surface to improve the ionization of surface molecules (Altelaar *et al.* 2006). ToF-SIMS analyses were conducted in the Materials Research Laboratory facilities at the University of Illinois at Urbana-Champaign (UIUC); specifically, the instrument used was a TRIFT ToF-SIMS mass spectrometer (Physical Electronics, Chanhassen, MN) equipped with a gold liquid metal ion source. The primary ion beam used Au_1 running at 22 keV, 2 nAmp, and the primary ion dose was kept below the static limit of 1×10^{13} primary ions cm^{-2} and negative secondary ions collected. Mass spectrometric images were collected using WinCadence software (Physical Electronics, Chanhassen, MN) with its built-in mosaic function, except HVC which was collected as two 600 × 600 μm images. Images measuring 1 × 1 mm were composed of 16 steps, each interrogating 250 × 250 μm; the areas of 1.5 × 1.5 mm also were composed of 16 steps, now measuring 375 × 375 μm each. Images containing HVC and AL were stitched as previously described

(Amaya et al. 2007). Individual images are composed of 256 × 256 pixels with each pixel representing a unique mass spectrum of the sample surface. All images were convolved once using the default settings in WinCadence and individually scaled to a relative intensity scale of 0 - 100%. Where multiple ToF-SIMS images are shown to compare distributions of different molecules within a single song nucleus, all images are from the same individual tissue section. Qualitative descriptions of histological patterns described in Results are based on observations made in all three adult males, though only a single representative section is shown in each figure. Where additional procedures were performed (i.e., cresyl violet, IHC) these were performed on sections serially adjacent to the section used for ToF-SIMS.

After determining the likely fatty acids based on mass matching, our putative identifications relied on comparing the spectra from the brain tissue with spectra from standards purchased either from Sigma-Aldrich or Cayman Chemical (> 95% purity). Standards were either adhered to or deposited on carbon tape and subjected to ToF-SIMS analysis and their mass to charge ratio recorded (Table 1). We confirmed our assignments of these fatty acids in the brain using an alternative approach; more specifically, the region of interest was removed, lipids extracted, and fatty acids analyzed by GC-MS (Supplemental S1 and S2). To determine if esterified lipids undergo chemical fragmentation, a standard of phosphatidylethanolamine (PE) purity of ~ 98% (Sigma-Aldrich) was adhered to carbon tape and subjected to ToF-SIMS analysis (Supplemental S3).

Principle component analysis (PCA)

For multivariate statistical analysis, mass spectra from the song nuclei from three different males were collected by using the region of interest function (ROI) in WinCadence. The developmental comparison consisted of three different males, for each age group, with ToF-SIMS collected from five different 200 × 200 μm areas within RA. Spectra were box binned and normalized to carbon (*m/z* 12), a ubiquitous and biologically significant ion. Contaminating peaks and peaks <*m/z* 50 were excluded from data analysis. PCA was carried out using PLS_Tool box (Eigenvector Research, Inc. Wenatchee, WA), and data were preprocessed by autoscaling and transformed to a logarithmic scale ($\log_{10}$) to ensure high-intensity peaks were not overrepresented (Wagner *et al.* 2004).

Immunohistochemistry

Sections were removed from –80 °C storage and fixed with 4% paraformaldehyde (pH 7.3) for 5 min and washed three times with 0.025 M PBS (pH 7.0) for 5 min each time. Tissue was blocked for 1 h at room temperature in a humidity chamber with Image-iT FX signal enhancer (I36933, Invitrogen, Carlsbad, CA), followed by a TBS-TX (50 mM Tris HCl, pH 7.4, 150 mM NaCl, and 0.1% Triton-X-100) wash (5 min, × 3). A second blocking step with TBS-TX plus 10% normal donkey serum was done, followed by a TBS-TX wash step.

Sections were then incubated with primary antibodies against the neuronal marker, NeuN 1:500, (MAB377, Millipore, Billerica, MA) and myelin basic protein, MBP 1:75, (AB9348, Millipore) at room temperature in a humidity chamber. After 1 hr tissues were washed with TBS-TX and incubated 1 hr with the secondary antibodies Alexa 488 (A-21202, Invitrogen) and Alexa 546 (A11040, Invitrogen) diluted 1:500, followed by a TBS-TX wash. Cell nuclei were stained with DAPI (12 μg/mL) for 5 min, washed with TBS-TX, and cover slip mounted with ProLong Gold (P36934, Invitrogen). Slides were then analyzed under a Zeiss Axiovert 200M (Carl Zeiss Microimaging, Inc., Thornwood, NY) fluorescence microscope on site at the Institute for Genomic Biology core facilities, UIUC.

Results

Fatty acids distinguish the major song nuclei

From ToF-SIMS data for each brain section examined (n=3 birds), images were constructed for 13 fatty acids and cholesterol. Using the ROI function, relative concentrations were assessed within the five major song nuclei and the two major subdivisions of the AL (Table 2). By ANOVA, there were significant differences among these brain regions for nine of these lipids, with the largest effect (nearly four-fold) observed for the long polyunsaturated EFA, arachidonic acid (ARA, 20:4 n-6).

Individual song nuclei were readily distinguishable from the surrounding brain tissue by their content of these lipids. Figure 2 presents an overview of the relative content of these lipids in nucleus RA compared to the surrounding arcopallium and nidopallium, in a single tissue section (images of additional song nuclei and at larger magnification are presented in Supplemental S4-S6). As reference and for comparison to conventional histological methods, adjacent sections were stained using cresyl violet and immunohistochemistry. Cresyl violet staining (Fig. 2B) shows this well-defined song nucleus sitting within the arcopallium and just below (ventral to) the nidopallium. Immunohistochemical labeling with the neuronal marker NeuN (Fig. 2C, green) shows robust labeling of the RA and significant labeling in the nidopallium, but little to no staining in the surrounding arcopallium. Myelin labeling (Fig. 2C, red) shows a clear demarcation and a more intense overall labeling of the RA compared to the arcopallium or nidopallium. Punctate areas of intense labeling in the anterior part of the arcopallium likely correspond to fiber tracks connecting RA to fasciculus prosencephali lateralis, and striations in the nidopallium are neuronal projections that connect the HVC and RA. The labeling of cell nuclei with DAPI (blue) shows no discernable difference in cell density across the image. ToF-SIMS analysis of palmitic acid (16:0) produces a striking image as this lipid is sharply enriched within the boundaries of nucleus RA, with intermediate labeling in the surrounding arcopallium and lower labeling in the overlying nidopallium (Fig. 2D). Fig. 2E summarizes the relative signal intensities for all 13 fatty acids and cholesterol in RA compared to surrounding tissue in this same brain section.

Variable content of Essential Fatty Acids in the song control system

The omega-3 and omega-6 unsaturated EFAs are of particular interest given their importance in cell signaling, brain function, and therapeutics. A survey of the local distributions of these in and around the six song system regions is presented in Figure 3. (Selected images are also shown aligned with reference sections in Supplemental S4. A similar series is shown for non-essential fatty acids in Supplemental S6). Eicosapentaenoic acid (EPA, 20:5 n-3) and arachidonic acid (ARA, 20:4 n-6) are notably reduced in the RA, especially in comparison to the nidopallium (Fig. 3C, D). In contrast, docosahexaenoic acid (DHA, 22:6 n-3) shows increased relative levels in the RA compared to surrounding tissue, as do the EFAs linoleic acid (18:2 n-6) and 11,14-eicosadienoic acid (20:2 n-6). The EFAs 8,11,14, eicosatrienoic acid (20:3 n-6) and adrenic acid (22:4 n-6) are not included in the figure as they show no difference in spatial distributions within these nuclei compared to the surrounding tissue, even though they do show differences in levels within different song nuclei (Table 2). Nucleus LMAN, which projects to RA, and its thalamic afferent (DLM) are generally similar to RA for all these EFAs. HVC also projects to RA, but HVC generally shows less differential content of the EFAs compared to surrounding tissue, with little or no enrichment for linoleic acid nor a reduction in ARA. Area X shows little differential content except for a reduction in ARA. The AL shows evidence of internal subdivisions according to the different distributions of EPA, DHA and ARA.

Subdivisions of LMAN revealed

The song control nucleus LMAN is essential for song learning, and has been described as having a central core of magnocellular neurons surrounded by a shell of parvicellular neurons, with discrete functions proposed for these two subregions (Johnson *et al.* 1995, Bottjer & Altenau 2010). We noted variation in the anatomical pattern of several lipids across this nucleus and analyzed this in further detail by line scan. ToF-SIMS imaging of the LMAN indicates reciprocal internal distributions of the monounsaturated 18-carbon fatty acid, oleic acid, and the fully saturated form, stearic acid (Fig. 4A, B). Linescan analysis, moving across the images from the upper left to the lower right, quantifies these distributions at each pixel (Fig. 6C). Oleic acid (red line) shows a significant increase in relative signal intensity in the area corresponding to the core of the nucleus. Stearic acid (blue line) shows two spots of maximum signal intensity extending over an area of ~150 μm (Fig. 6C). Both areas of increased stearic acid signal are immediately adjacent to the increased oleic acid signal. Comparing the two images it appears the increased stearic acid signal encircles the increased oleic acid signal (Fig. 6A, B). This is consistent with the prior descriptions of core/shell regions (Johnson *et al.* 1995, Bottjer & Altenau 2010). Direct overlap of IHC and ToF-SIMS images from adjacent sections (not shown) indicates the lipids are concentrated mostly outside of neuronal nuclei but we cannot discriminate whether they are present in glia or neuropil.

Discrimination of song nuclei by PCA

The observations above reveal that known chemicals individually show clear differences in distribution across the major song nuclei. We used PCA to analyze at once the entire set of SIMS spectra from each of the three birds, considering all five song nuclei plus NCM and CMM in the AL (Fig. 5). Principle component 1 (PC1, x-axis) captures 55% of the variation in the data. Much of the variation is between the chemical profiles of the NCM/CMM and RA, along with one spectrum from the LMAN (Fig. 5A). Analysis of the corresponding loadings plot (Fig. 5B) reveals that the NCM/CMM region has the greatest association (increased relative amount) with *m/z* 79 (phosphate), *m/z* 122 (ethanolamine), and three unknown peaks (*m/z* 81, 153, 124). The same loadings plot shows that the RA and one LMAN spectrum have a relative increase in peaks corresponding to four fatty acids: *m/z* 255 (palmitic acid), *m/z* 227 (myristic acid), *m/z* 309 (11-eicosenoic acid), and *m/z* 327 (DHA) as compared to the NCM/CMM. Spectra from the other song nuclei show little variation in relation to the NCM/CMM and RA based on their position near the x-axis. Principle component 2 (PC2, y-axis) accounts for 16.44% of the variation and captures major differences between striatal nucleus AreaX and the thalamic song nucleus DLM, along with some spectra from the RA and LMAN (Fig. 5A). Much of the difference is captured by an unknown peak, *m/z* 124, showing relative abundance in AreaX. Other peaks highly associated with AreaX include *m/z* 565, *m/z* 163, *m/z* 153, *m/z* 63, *m/z* 79 (phosphate) and *m/z* 122 (representing phosphoethanolamine) (Fig. 5B). Along PC2 of the corresponding loadings plot, peaks corresponding to *m/z* 327 (DHA), *m/z* 309 (11-eicosenoic acid), *m/z* 283 (stearic acid), and *m/z* 281 (oleic acid) show higher relative levels in the DLM and some spectra from the RA and LMAN as compared to AreaX (Fig. 5). Spectra from the NCM, CMM, HVC, and some RA tissue show little variation compared to the DLM and AreaX based on their proximity to the y-axis (Fig. 5A).

Developmental changes in the RA

We examined male birds at three different ages, corresponding to just before onset of the critical period for song learning and circuit maturation (post-hatch day 20, p20), the peak of the critical period (p40) and adulthood (>p90). PCA comparing RAs from three male birds at each age shows significant separation between adult and p20 RAs (Fig. 6A); in contrast comparing SIMS data collected from 5 unique areas within each RA shows less variation.

Most of the age-related separation is along PC2, accounting for 21.26% of the total variation in the spectral data, while PC1 accounts for 66.25% of the variation and appears to capture inherent biological variation (Fig. 6A). Analysis of the corresponding loadings plot for PC2 reveals that *m/z* 79 (phosphate), *m/z* 124 (unknown), and *m/z* 122 (phosphoethanolamine) are the major peaks associated (increased relative abundance) with RAs from p20 birds compared to adults (Fig. 6B). The loadings plot also shows that RAs from adult birds show greatest association (relative abundance) with high molecular peaks *m/z* >800, along with some fatty acids including: DHA (*m/z* 327), 11-eicosenoic acid (*m/z* 309), and stearic acid (*m/z* 283), in addition to a peak previously identified as vitamin E (*m/z* 429) (Fig. 6B).

Discussion

ToF-SIMS is a sensitive surface analysis method relying on the bombardment of a primary ion to analyze the top few layers of a sample surface (Sodhi 2004). In the past, extensive chemical fragmentation has limited its application for imaging larger molecules from biological tissues; however this limitation has been ameliorated by using cluster ion sources (Brunelle *et al.* 2005) and higher molecular weight primary ions (Fletcher *et al.* 2006). The results presented here confirm the use of ToF-SIMS as a valuable tool used to uncover chemical heterogeneity and the local distributions of fatty acids within the complex anatomy of brain tissue sections. It may also complement conventional histological and immunocytochemical staining procedures for analysis of brain anatomy, as we have shown here using the zebra finch song control system, finding new neuroanatomical features not evident with these other techniques.

A key feature of ToF-SIMS imaging is both a strength and a weakness: it can image the distribution of any peak detected by mass spectroscopy, without requiring any pre or post hoc knowledge of the chemical responsible for the peak. Assignment of chemical identities to specific masses is challenging as there is no comprehensive molecular ion database for ToF-SIMS; moreover, ionization patterns potentially vary within different subregions of the same tissue section based on variation in the local chemical makeup (Ostrowski *et al.* 2005). Topographical features can also affect sputtering of secondary ions (McDonnell *et al.* 2005); however, our use of cryosectioning minimizes these problems. Although our mass assignments must be qualified as putative, many of them were supported by direct ToF-SIMS analysis of known standards (Table 1) and by GC-MS analysis (Supplemental S1 and S2).

We believe the majority of the fatty acids detected in this study are probably derived from esterified lipids that fragmented upon impact of the primary ion. In support of this, we observed that a pure standard of phosphatidylethanolamine (PE) gave rise primarily to free fatty acids upon ToF-SIMS analysis (Supplemental S3). We also considered the possibility that the signals for the unsaturated EFAs ARA and EPA could have been confounded due to fragmentation. However, we believe these signals represent distinct chemical species present in the tissue since both species were detected in forebrain samples by gas chromatography mass spectrometry (Supplemental S2), and standards subjected to ToF-SIMS exhibited minimal and non-identical patterns of fragmentation (data not shown).

We constructed images showing the simultaneous distributions within individual sections of zebra finch brain for each of 13 well-defined lipids and cholesterol. The anatomical patterns of the various fatty acids generally respected boundaries within the tissue evident by cresyl violet staining or specific immunohistochemistry, though in some cases additional details were evident that were not apparent by these other methods (e.g., Fig. 2D). For example, we noted complementary patterns of several fatty acids associated with song nucleus LMAN, consistent with the presence of distinct “core” and “shell” subregions previously defined by

their distinct neuroanatomical projections (Johnson et al. 1995) and different effects of lesion (Bottjer & Altenau 2010). In our data, both of these subregions show enrichment for the saturated 18-carbon fatty acid stearic acid, whereas the shell only is markedly enriched in the monounsaturated form, oleic acid.

In general our results show that each song nucleus can be distinguished by its relative complement of fatty acids, with respect both to the surrounding tissue (Figs. 2 and 3) and to the other song nuclei (Table 2), an observation that parallels findings using microarrays and in situ hybridization to measure specific mRNA content (Lovell *et al.* 2008). We replicated our observations in 3 different adult zebra finch brains, and observed a statistically significant main effect of brain region on signal for 8 of the 14 compounds we explicitly quantified (Table 2). We also used PCA on the entire spectral data set, finding that each song nucleus is discriminated fairly effectively in the first two principal components (Fig. 5). PCA is an unsupervised statistical approach used to reduce large complex chemical data sets into a few manageable variables. It can efficiently extract information representing chemical differences and similarities between samples (Lindon *et al.* 2007) and has been used in SIMS previously (Sjovall *et al.* 2004, Wu *et al.* 2007, Kulp *et al.* 2006). The clustering of our data according to song nucleus is especially interesting given that our zebra finches are not inbred and still retain robust genetic diversity (Forstmeier et al., 2007). PC1 captures 55% of the spectral variation and seems to segregate the brain regions according sensory versus motor function in the song system. The NCM/CMM is a sensory region that shows significant chemical differences when compared with the RA, which is the motor output nucleus of the telencephalic control system. In contrast, the DLM, HVC, LMAN, and AreaX regions are more clearly involved in both sensory and motor function, and cluster between the RA and NCM/CMM areas. The loadings plot shows a decreased association of the RA, compared to the NCM/CMM, with phosphate and ethanolamine, which may suggest a relative increase in sphingomyelin and glycosphingolipids in the RA (Isaac *et al.* 2006, Sastry 1985). Along PC2, the major effect is the segregation of the striatal nucleus Area X from the other song regions. Interestingly, AreaX also has a rather different profile of gene expression in the combined microarray studies of the SoNG Initiative (Replogle *et al.* 2008) (and unpublished).

EFAs and song nucleus RA

EFAs are of particular interest given their known roles in cellular signaling and plasticity, and the fact that they are not synthesized locally but must be selectively accumulated from circulating stores derived from dietary sources. The EFAs showed especially marked distribution patterns in song nucleus RA. DHA is notably increased in the RA compared to surrounding brain regions. It is believed that the highly unsaturated nature of DHA provides significant membrane fluidity, required for proper brain function (Bourre et al. 1992) and neuronal development (Calderon & Kim 2004), and a protective role against neurodegenerative disease has been suggested (Oster & Pillot 2010). In other systems, DHA has been shown to be enriched in metabolically active brain areas such as the mammalian basal ganglia and gray matter (Diau et al. 2005), in brain regions with increased synaptic vesicles (McGee et al. 1994), and in nerve growth cones (Martin & Bazan 1992). RA itself has a high level of metabolic activity (Adret & Margoliash 2002) with dense synaptic input from two sources (HVC and LMAN) and a mixture of glutamatergic projection neurons and GABAergic interneurons (Pinaud & Mello 2007).

In contrast to DHA, two other EFAs implicated in brain function, EPA and ARA, are decreased in RA. EPA is a precursor to DHA, suggesting the possibility that RA neurons favor synthesis of DHA at the expense of EPA. ARA is a polyunsaturated fatty acid with multiple roles in cell signaling and synaptic potentiation (Williams et al. 1989), but it also exhibits pro-inflammatory effects by acting as a precursor in eicosanoid synthesis

(Simopoulos 2002) and may mediate processes leading to neurodegenerative disease (Sanchez-Mejia & Mucke 2010). Intriguingly, the alpha-synuclein protein (SNCA) is also notably decreased in the RA of the adult zebra finch (George et al. 1995, Jin & Clayton 1997), and it interacts closely with ARA (Darios *et al.* 2010) and has reciprocal effects on the metabolism of ARA versus DHA (Golovko *et al.* 2007, Golovko *et al.* 2009). These observations suggest a concerted regulation within RA of particular lipid pathways that mediate cellular integrity and synaptic plasticity.

In the remaining song regions we also measured localized decreases in ARA, with two exceptions, Area X and the AL (NCM/CMM). AreaX is located in the striatum proper of the basal ganglia and contains both striatal and pallidal neurons, which are composed of mostly small γ-aminobutyric acid (GABA)ergic spiny neurons with fewer large GABAergic neurons (Farries & Perkel 2002, Reiner *et al.* 2004, Grisham & Arnold 1994, Carrillo & Doupe 2004). AL has a complex internal organization and is the central auditory area engaged in song perception; it shows high levels of both ARA and EPA, especially in the caudal part of the NCM subregion (Fig. 3, Supplemental S5). The AL also shows unique distributions for palmitic acid, stearic acid, and oleic acid (Supplemental S5). Molecular studies of the AL have shown retinoic acid receptors with a similar expression pattern as the distribution of ARA, EPA, and stearic acid (Jeong *et al.* 2005). Retinoic acid production in the song control system is necessary for normal song maturation (Denisenko-Nehrbass et al. 2000), and in mice it has a role in neuronal plasticity and learning and memory (Krezel *et al.* 1998, Cocco *et al.* 2002). The differential distribution of fatty acids may reflect distinct cellular populations in the auditory caudomedial telencephalon, with distinct molecular, anatomical, and physiological properties.

Fatty acid changes during the song learning period

A male zebra finch learns to sing during a discrete “critical period” in late juvenile life. Importantly, the entire song learning process occurs after development is otherwise largely complete and the bird has fledged from the nest. A young male first begins to produce immature vocalizations at about P30, the age at which axons abruptly project from nucleus HVC and form synaptic connections onto the major output nucleus of the telencephalic control system (Fig. 1), nucleus RA (Konishi & Akutagawa 1985, Holloway & Clayton 2001). The bird's vocal performance gradually becomes more refined and stereotyped over the next 4-8 weeks, reaching its mature adult form by ~P90, after which no further change in the song will occur for the rest of the bird's life.

We applied ToF-SIMS to ask whether there were significant differences in lipid composition in nucleus RA before (P20), during (P40), and after (adult) the developmental song learning period. Unlike direct analysis of anatomical distributions observed within individual brain sections, comparisons of sections taken from different animals must confront the potential for artifacts arising from subtle variations in sample preparation. To minimize this risk we used a minimal approach to sample preparation, with the sections simply frozen and then vacuum dried prior to sputter coating, and then employed PCA as a way to objectively include all the spectral data in this analysis (Fig. 6).

Just as our PCA analysis showed a major effect of brain region (Fig. 5), here PCA revealed a major effect of developmental age on the spectral patterns obtained from nucleus RA, especially along the axis of the second principal component (Fig. 6). PC2 separates p20 and adult RAs, with RAs from p40 birds exhibiting an apparent chemical transition from p20 to adults. The P40 samples in particular show variation along PC2, intermediate between the two extremes of the P20 and adult samples. This variation is suggestive of (and may be related to) the variable progress that different individuals are making in their song development at this age (Tchernichovski et al., 2001). The corresponding loadings plot

shows a relative increase in high molecular weight ions (*m/z* ~800–860) in the adult RA compared to the p20 RAs. Although these have not been positively identified, they may represent esterified lipids such as triglycerides and glycosphingolipids (Pernber *et al.* 2007, Touboul *et al.* 2005). In addition to higher levels of many fatty acids in adult RAs (i.e., DHA and 11-eicosenic acid), a peak previously identified as vitamin E (*m/z* 429) (Monroe *et al.* 2005) also shows relative higher levels in RAs from adult birds; in this case, however, we do not observe several characteristic SIMS fragmentation ions as previously observed. Increased vitamin E levels have been shown during development of mammalian brains (Zhang *et al.* 1996). Myelination in the RA has previously been identified as taking place around p50 (Clayton 1997). Therefore, we expect to see higher relative levels of phosphate-containing lipids in p20 RAs compared to adults. Other ions (*m/z* <150) show significant association with p20 RAs and likely represent fragmentation ions of larger molecules, making their identification difficult.

Prospects

The subcellular imaging of fatty acids and other small molecules by ToF-SIMS in brain sections opens significant avenues in the study of neurochemistry and disease, especially when applied in an animal model like the zebra finch. Future studies to focus on the identification of unknown peaks in the ToF-SIMS spectra will significantly aid our understanding of small molecule heterogeneities across the zebra finch song system and their prospective biological importance in brain development and learning and memory.

Supplementary Material

Refer to Web version on PubMed Central for supplementary material.

Acknowledgments

We thank Timothy Spila for his assistance with the ToF-SIMS and Alexander Ulanov with the GC-MS. This investigation was supported by the National Institutes of Health (NIH) under a Ruth L. Kirschstein National Research Service Award No. F31 NS060179-01A1 to KRA, by Award No. R01 DE018866 from the National Institute of Dental and Craniofacial Research (NIDCR) and the Office of Director, NIH, and by Award No. P30 DA018310 from the National Institute On Drug Abuse (NIDA) to JVS, and Award No. PHS 2 R01 NS051820 to DFC. Research was carried out in part in the Frederick Seitz Materials Research Laboratory Central Facilities, University of Illinois at Urbana-Champaign, which are partially supported by the U.S. Department of Energy (DOE) under Award Nos. DE-FG02-07ER46453 and DE-FG02-07ER46471. This work is adapted from the doctoral dissertation (University of Illinois) of Kensey R. Amaya. The content is solely the responsibility of the authors and does not necessarily represent the official views of the NIDCR, NIDA, NIH or the DOE.

Abbreviations

ToF-SIMS	time-of-flight-secondary ion mass spectrometry
RA	robust nucleus of the arcopallium
CMM	caudal medial mesopallium
DLM	dorsomedial division of the medial thalamus
LMAN	lateral magnocellular nucleus of the anterior nidopallium
NCM	caudal medial nidopallium
AL	auditory lobule
EFA	essential fatty acid
DHA	docosahexaenoic acid

ARA	arachidonic acid
EPA	eicosapentaenoic acid
PCA	principle component analysis

References

Adret P, Margoliash D. Metabolic and neural activity in the song system nucleus robustus archistriatalis: effect of age and gender. J. Comp. Neurol. 2002; 454:409–423. [PubMed: 12455006]

Altelaar AFM, Klinkert I, Jalink K, de Lange RPJ, Adan RAH, Heeren RMA, Piersma SR. Gold-enhanced biomolecular surface imaging of cells and tissue by SIMS and MALDI mass spectrometry. Anal. Chem. 2006; 78:734–742. [PubMed: 16448046]

Amaya KR, Monroe EB, Sweedler JV, Clayton DF. Lipid imaging in the zebra finch brain with secondary ion mass spectrometry. Int. J. of Mass Spectrom. 2007; 260:121–127.

Bazan NG. Lipid signaling in neural plasticity, brain repair, and neuroprotection. Mol. Neurobiol. 2005; 32:89–103. [PubMed: 16077186]

Bottjer SW, Altenau B. Parallel pathways for vocal learning in basal ganglia of songbirds. Nat. Neurosci. 2010; 13:153–155. [PubMed: 20023650]

Bourre JM, Dumont OS, Piciotti MJ, Pascal GA, Durand GA. Dietary alpha-linolenic acid deficiency in adult rats for 7 months does not alter brain docosahexaenoic acid content, in contrast to liver, heart and testes. Biochim. Biophys. Acta. 1992; 1124:119–122. [PubMed: 1347458]

Brenowitz EA, Margoliash D, Nordeen KW. An introduction to birdsong and the avian song system. J. Neurobiol. 1997; 33:495–500. [PubMed: 9369455]

Brunelle A, Touboul D, Laprevote O. Biological tissue imaging with time-of-flight secondary ion mass spectrometry and cluster ion sources. J. Mass Spectrom. 2005; 40:985–999. [PubMed: 16106340]

Calderon F, Kim HY. Docosahexaenoic acid promotes neurite growth in hippocampal neurons. J. Neurochem. 2004; 90:979–988. [PubMed: 15287904]

Carrillo GD, Doupe AJ. Is the songbird Area X striatal, pallidal, or both? An anatomical study. J. Comp. Neurol. 2004; 473:415–437. [PubMed: 15116398]

Clayton DF. Role of gene regulation in song circuit development and song learning. J. Neurobiol. 1997; 33:549–571. [PubMed: 9369459]

Clayton DF, George JM. Synucleins in synaptic plasticity and neurodegenerative disorders. J. Neurosci. Res. 1999; 58:120–129. [PubMed: 10491577]

Clayton DF, Balakrishnan CN, London SE. Integrating genomes, brain and behavior in the study of songbirds. Curr. Biol. 2009; 19:865–873.

Cocco S, Diaz G, Stancampiano R, Diana A, Carta M, Curreli R, Sarais L, Fadda F. Vitamin A deficiency produces spatial learning and memory impairment in rats. Neuroscience. 2002; 115:475–482. [PubMed: 12421614]

Cole-Edwards KK, Bazan NG. Lipid signaling in experimental epilepsy. Neurochem. Res. 2005; 30:847–853. [PubMed: 16187219]

Darios F, Ruipérez V, López I, Villanueva J, Gutierrez LM, Davletov B. Alpha-Synuclein sequesters arachidonic acid to modulate SNARE-mediated exocytosis. EMBO Reports. 2010; 11:528–533. [PubMed: 20489724]

Davletov B, Montecucco C. Lipid function at synapses. Curr. Opin. Neurobiol. 2010; 20:543–549. [PubMed: 20655194]

Denisenko-Nehrbass NI, Jarvis E, Scharff C, Nottebohm F, Mello CV. Site-specific retinoic acid production in the brain of adult songbirds. Neuron. 2000; 27:359–370. [PubMed: 10985355]

Diau GY, Hsieh AT, Sarkadi-Nagy EA, Wijendran V, Nathanielsz PW, Brenna JT. The influence of long chain polyunsaturate supplementation on docosahexaenoic acid and arachidonic acid in baboon neonate central nervous system. BMC Med. 2005; 3:11. [PubMed: 15975147]

Ewing AG. Molecule specific imaging in biology: What are the challenges and the important applications? Appl. Surf. Sci. 2006; 252:6821–6826.

Farries MA, Perkel DJ. A telencephalic nucleus essential for song learning contains neurons with physiological characteristics of both striatum and globus pallidus. J. Neurosci. 2002; 22:3776–3787. [PubMed: 11978853]

Fenton WS, Hibbeln J, Knable M. Essential fatty acids, lipid membrane abnormalities, and the diagnosis and treatment of schizophrenia. Biol. Psychiatry. 2000; 47:8–21. [PubMed: 10650444]

Fletcher JS, Conlan XA, Jones EA, Biddulph G, Lockyer NP, Vickerman JC. TOF-SIMS analysis using C-60- effect of impact energy on yield and damage. Anal. Chem. 2006; 78:1827–1831. [PubMed: 16536417]

Forstmeier W, Segelbacher G, Mueller JC, Kempenaers B. Genetic variation and differentiation in captive and wild zebra finches (Taeniopygia guttata). Mol Ecol. 2007; 16:4039–4050. [PubMed: 17894758]

George JM, Jin H, Woods WS, Clayton DF. Characterization of a novel protein regulated during the critical period for song learning in the zebra finch. Neuron. 1995; 15:361–372. [PubMed: 7646890]

Golovko MY, Rosenberger TA, Feddersen S, Faergeman NJ, Murphy EJ. Alpha-Synuclein gene ablation increases docosahexaenoic acid incorporation and turnover in brain phospholipids. J. Neurochem. 2007; 101:201–211. [PubMed: 17250657]

Golovko MY, Barceló-Coblijn G, Castagnet PI, Austin S, Combs CK, Murphy EJ. The role of alpha-synuclein in brain lipid metabolism: A downstream impact on brain inflammatory response. Mol. Cell. Biochem. 2009; 326:55–66. [PubMed: 19116775]

Grisham W, Arnold AP. Distribution of Gaba-Like Immunoreactivity in the Song System of the Zebra Finch. Brain Res. 1994; 651:115–122. [PubMed: 7922557]

Hartmann T, Kuchenbecker J, Grimm MO. Alzheimer's disease: the lipid connection. J. Neurochem. 2007; 103(Suppl 1):159–170. [PubMed: 17986151]

Holloway CC, Clayton DF. Estrogen synthesis in the male brain triggers development of the avian song control pathway in vitro. Nat. Neurosci. 2001; 4:170–175. [PubMed: 11175878]

Innis SM. Dietary omega 3 fatty acids and the developing brain. Brain Res. 2008; 1237:35–43. [PubMed: 18789910]

Isaac G, Pernber Z, Gieselmann V, Hansson E, Bergquist J, Mansson JE. Sulfatide with short fatty acid dominates in astrocytes and neurons. FEBS J. 2006; 273:1782–1790. [PubMed: 16623713]

Israeli E, Sharon R. Beta-synuclein occurs in vivo in lipid-associated oligomers and forms hetero-oligomers with alpha-synuclein. J. Neurochem. 2009; 108:465–474. [PubMed: 19012742]

Jeong JK, Velho TAF, Mello CV. Cloning and expression analysis of retinoic acid receptors in the zebra finch brain. J. Comp. Neurol. 2005; 489:23–41. [PubMed: 15977168]

Jin H, Clayton DF. Synelfin regulation during the critical period for song learning in normal and isolated juvenile zebra finches. Neurobiol. Learn. Mem. 1997; 68:271–284. [PubMed: 9398589]

Johansson B. ToF-SIMS imaging of lipids in cell membranes. Surf. Interface Anal. 2006; 38:1401–1412.

Johnson F, Sablan MM, Bottjer SW. Topographic organization of a forebrain pathway involved with vocal learning in zebra finches. J. Comp. Neurol. 1995; 358:260–278. [PubMed: 7560286]

Kim K, Yang J, Kim E. Diacylglycerol kinases in the regulation of dendritic spines. Journal of Neurochemistry. 2010; 112:577–587. [PubMed: 19922438]

Konishi M, Akutagawa E. Neuronal growth, atrophy and death in a sexually dimorphic song nucleus in the zebra finch brain. Nature. 1985; 315:145–147. [PubMed: 3990816]

Krezel W, Ghyselinck N, Abdel T, Dupe V, Kastner P, Borelli E, Chambon P. Impaired locomotion and dopamine signaling in retinoid receptor mutant mice. Eur. J. Neurosci. 1998; 10:370–370.

Kulp KS, Berman ES, Knize MG, Shattuck DL, Nelson EJ, Wu L, Montgomery JL, Felton JS, Wu KJ. Chemical and biological differentiation of three human breast cancer cell types using time-of-flight secondary ion mass spectrometry. Anal. Chem. 2006; 78:3651–3658. [PubMed: 16737220]

Lindon, JC.; Nicholson, JK.; Holmes, E. The handbook of metabonomics and metabolomics. Elsevier; Amsterdam ; Oxford: 2007.

London SE, Monks DA, Wade J, Schlinger BA. Widespread capacity for steroid synthesis in the avian brain and song system. Endocrinology. 2006; 147:5975–5987. [PubMed: 16935847]

Lovell PV, Clayton DF, Replogle KL, Mello CV. Birdsong “Transcriptomics”: Neurochemical Specializations of the Oscine Song System. Plos One. 2008; 3:e3440. [PubMed: 18941504]

Maier O, Oberle V, Hoekstra D. Fluorescent lipid probes: some properties and applications (a review). Chem. Phys. Lipids. 2002; 116:3–18. [PubMed: 12093532]

Martin RE, Bazan NG. Changing fatty acid content of growth cone lipids prior to synaptogenesis. J. Neurochem. 1992; 59:318–325. [PubMed: 1613507]

Mas S, Perez R, Martinez-Pinna R, Egido J, Vivanco F. Cluster TOF-SIMS imaging: a new light for in situ metabolomics? Proteomics. 2008; 8:3735–3745. [PubMed: 18712766]

McDonnell LA, Piersma SR, Altelaar AFM, Mize TH, Luxembourg SL, Verhaert PDEM, van Minnen J, Heeren RMA. Subcellular imaging mass spectrometry of brain tissue. J. Mass Spectrom. 2005; 40:160–168. [PubMed: 15706616]

McGee CD, Greenwood CE, Cinader B. Dietary fat composition and age affect synaptosomal and retinal phospholipid fatty acid composition in C57BL/6 mice. Lipids. 1994; 29:605–610. [PubMed: 7815894]

Mello C, Nottebohm F, Clayton D. Repeated exposure to one song leads to a rapid and persistent decline in an immediate early gene's response to that song in zebra finch telencephalon. J. Neurosci. 1995; 15:6919–6925. [PubMed: 7472448]

Mello CV. Mapping vocal communication pathways in birds with inducible gene expression. J. Comp. Physiol. A Neuroethol. Sens. Neural Behav. Physiol. 2002; 188:943–959. [PubMed: 12471493]

Monroe EB, Jurchen JC, Lee J, Rubakhin SS, Sweedler JV. Vitamin E imaging and localization in the neuronal membrane. J. Am. Chem. Soc. 2005; 127:12152–12153. [PubMed: 16131155]

Monroe EB, Annangudi SP, Hatcher NG, Gutstein HB, Rubakhin SS, Sweedler JV. SIMS and MALDI MS imaging of the spinal cord. Proteomics. 2008; 8:3746–54. [PubMed: 18712768]

Moriguchi T, Greiner RS, Salem N Jr. Behavioral deficits associated with dietary induction of decreased brain docosahexaenoic acid concentration. J. Neurochem. 2000; 75:2563–2573. [PubMed: 11080210]

Nygren H, Malmberg P, Kriegeskotte C, Arlinghaus HF. Bioimaging TOF-SIMS: localization of cholesterol in rat kidney sections. FEBS Lett. 2004; 566:291–293. [PubMed: 15147911]

Oster T, Pillot T. Docosahexaenoic acid and synaptic protection in Alzheimer's disease mice. BBA-Mol. Cell Bio. L. 2010; 1801:791–798.

Ostrowski SG, Szakal C, Kozole J, Roddy TP, Xu JY, Ewing AG, Winograd N. Secondary ion MS imaging of lipids in picoliter vials with a buckminsterfullerene ion source. Anal. Chem. 2005; 77:6190–6196. [PubMed: 16194078]

Pernber Z, Richter K, Mansson JE, Nygren H. Sulfatide with different fatty acids has unique distributions in cerebellum as imaged by time-of-flight secondary ion mass spectrometry (TOF-SIMS). Biochim. Biophys. Acta. 2007; 1771:202–209. [PubMed: 17257892]

Pinaud R, Mello CV. GABA immunoreactivity in auditory and song control brain areas of zebra finches. J.Chem. Neuroanat. 2007; 34:1–21. [PubMed: 17466487]

Piomelli D. The molecular logic of endocannabinoid signalling. Nature Reviews Neuroscience. 2003; 4:873–884.

Reiner A, Laverghetta AV, Meade CA, Cuthbertson SL, Bottjer SW. An immunohistochemical and pathway tracing study of the striatopallidal organization of area X in the male zebra finch. J. Comp. Neurol. 2004; 469:239–261. [PubMed: 14694537]

Replogle K, Arnold AP, Ball GF, et al. The Songbird Neurogenomics (SoNG) Initiative: community-based tools and strategies for study of brain gene function and evolution. BMC Genomics. 2008; 9:131. [PubMed: 18366674]

Sanchez-Mejia RO, Mucke L. Phospholipase A2 and arachidonic acid in Alzheimer's disease. BBA-Mol. Cell Bio. L. 2010; 1801:784–790.

Sastry PS. Lipids of nervous tissue: composition and metabolism. Prog. Lipid Res. 1985; 24:69–176. [PubMed: 3916238]

Simopoulos AP. Omega-3 fatty acids in inflammation and autoimmune diseases. J. Am. Coll. Nutr. 2002; 21:495–505. [PubMed: 12480795]

Sjovall P, Lausmaa J, Johansson B. Mass spectrometric imaging of lipids in brain tissue. Anal. Chem. 2004; 76:4271–4278. [PubMed: 15283560]

Soderstrom K, Tian Q, Valenti M, Di Marzo V. Endocannabinoids link feeding state and auditory perception-related gene expression. J Neurosci. 2004; 24:10013–10021. [PubMed: 15525787]

Sodhi RNS. Time-of-flight secondary ion mass spectrometry (TOF-SIMS): versatility in chemical and imaging surface analysis. Analyst. 2004; 129:483–487. [PubMed: 15152322]

Suzuki T. Lipid rafts at postsynaptic sites: distribution, function and linkage to postsynaptic density. Neurosci. Res. 2002; 44:1–9. [PubMed: 12204288]

Tahallah N, Brunelle A, De La Porte S, Laprevote O. Lipid mapping in human dystrophic muscle by cluster-time-of-flight secondary ion mass spectrometry imaging. J. Lipid Res. 2008; 49:438–454. [PubMed: 18025000]

Tchernichovski O, Mitra PP, Lints T, Nottebohm F. Dynamics of the vocal imitation process: how a zebra finch learns its song. Science. 2001; 291:2564–2569. [PubMed: 11283361]

Touboul D, Brunelle A, Halgand F, De La Porte S, Laprevote O. Lipid imaging by gold cluster time-of-flight secondary ion mass spectrometry: application to Duchenne muscular dystrophy. J. Lipid Res. 2005; 46:1388–1395. [PubMed: 15834124]

Wagner MS, Graham DJ, Ratner BD, Castner DG. Maximizing information obtained from secondary ion mass spectra of organic thin films using multivariate analysis. Surf. Sci. 2004; 570:78–97.

Warren WC, Clayton DF, Ellegren H, et al. The genome of a songbird. Nature. 2010; 464:757–762. [PubMed: 20360741]

Williams JH, Errington ML, Lynch MA, Bliss TV. Arachidonic acid induces a long-term activity-dependent enhancement of synaptic transmission in the hippocampus. Nature. 1989; 341:739–742. [PubMed: 2571939]

Wu L, Lu X, Kulp KS, Knize MG, Berman ESF, Nelson EJ, Felton JS, Wu KJJ. Imaging and differentiation of mouse embryo tissues by ToF-SIMS. Int. J. of Mass Spectrom. 2007; 260:137.

Zeigler, HP.; Marler, P. Behavioral Neurobiology Of Bird Song (Annals of the New York Academy of Sciences, Vol. 1016). New York Academy of Sciences; 2004.

Zhang Y, Appelkvist EL, Kristensson K, Dallner G. The lipid compositions of different regions of rat brain during development and aging. Neurobiol. Aging. 1996; 17:869–875. [PubMed: 9363798]

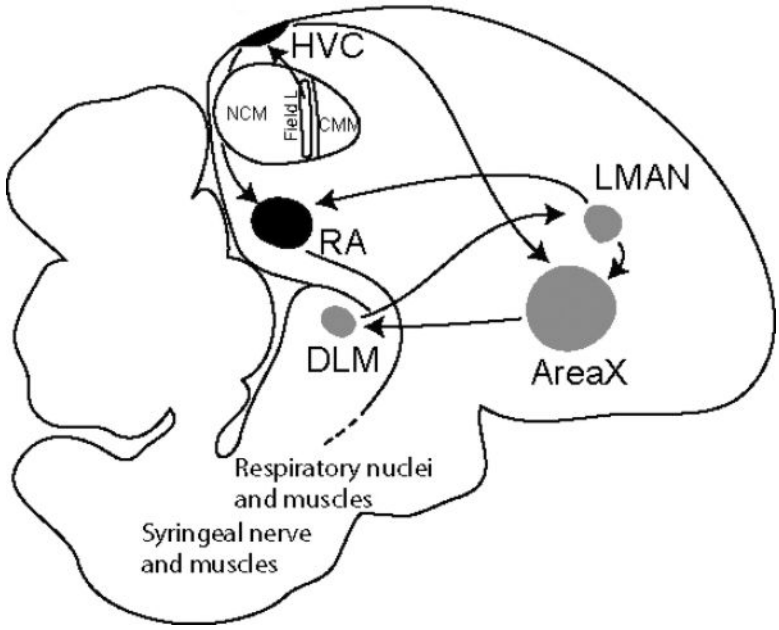

Figure 1.

Schematic drawing of a sagittal section of an adult male zebra finch brain showing the major song nuclei and neuronal connections of the song system. The anterior forebrain pathway, in grey, is composed of AreaX, the lateral magnocellular nucleus of the anterior nidopallium (LMAN), and the dorsomedial division of the medial thalamus (DLM). In white, the auditory pathway includes Field L, the caudal medial mesopallium (CMM), and the caudal medial nidopallium (NCM), which make up the auditory lobule (AL). In black, the song motor pathway is composed of the robust nucleus of the arcopallium (RA) and the HVC.

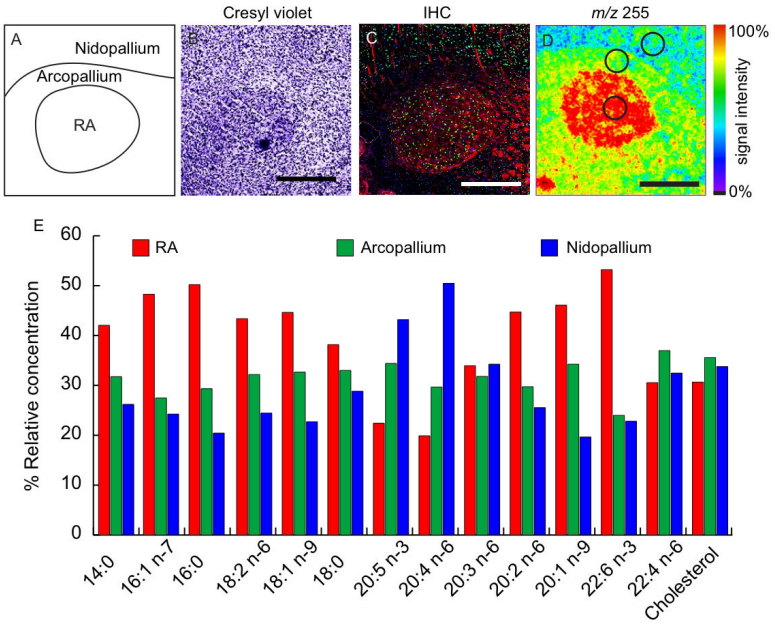

Figure 2.

Relative fatty acid concentration across an image of RA. **(A)** Illustration showing anatomical features across RA, **(B)** cresyl violet stained section showing cell distribution, **(C)** IHC showing cell distribution with DAPI (blue), neuronal distribution NeuN (green), myelin basic protein (red). **(D)** ToF-SIMS image showing the distribution of palmitic acid (16:0) across the RA. **(E)** The graph compares the relative concentration of different fatty acids between RA (red), the arcopallium (green), and nidopallium (blue). Spectra were collected by ROI, areas outlined in (D), normalized to the carbon ion, and expressed as a percentage of the total from the different regions of interest. Relative concentrations should only be compared between regions for a single fatty acid and not between fatty acids. Scale bar = 500 μm.

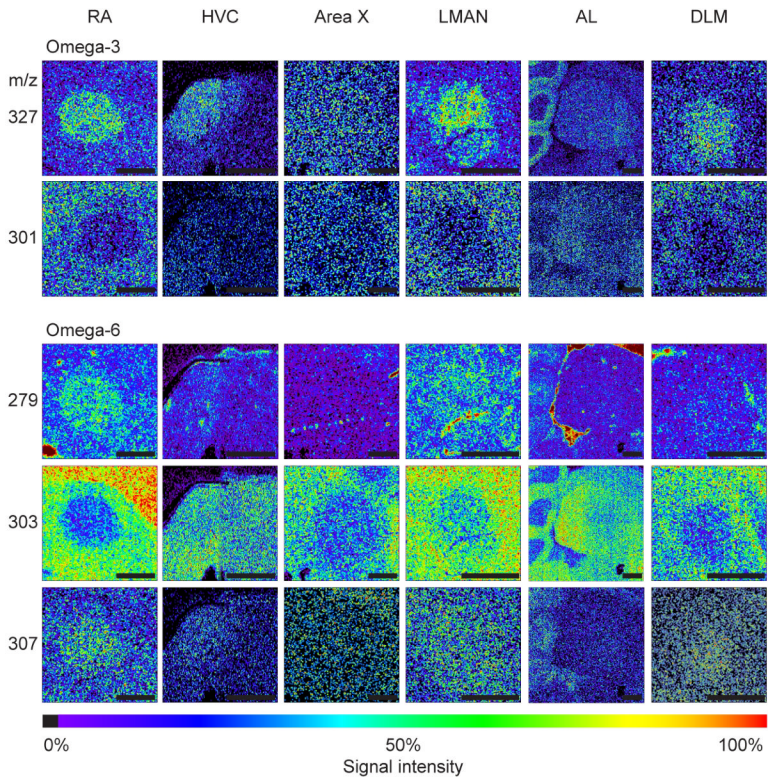

Figure 3.

ToF-SIMS images show the distribution of essential fatty acids collected across the song nuclei: RA, HVC, AreaX, LMAN, AL, and DLM. Omega-3 fatty acids—eicosapentaenoic acid (20:5 n-3, *m/z* 301), docosahexaenoic acid (22:6 n-3, *m/z* 327), and omega-6 fatty acids—linoleic acid (18:2 n-6, *m/z* 279), arachidonic acid (20:4 n-6, *m/z* 303), and docosadienoic acid (20:2 n-6, *m/z* 307). Images for 8,11,14-Eicosatrienoic acid (20:3 n-6), and adrenic acid (22:4 n-6) show no difference in spatial distribution across the song nuclei therefore were not included. All images have been scaled to a relative 0 - 100% intensity scale and their absolute ion count number may be different. Scale bar = 500 μm.

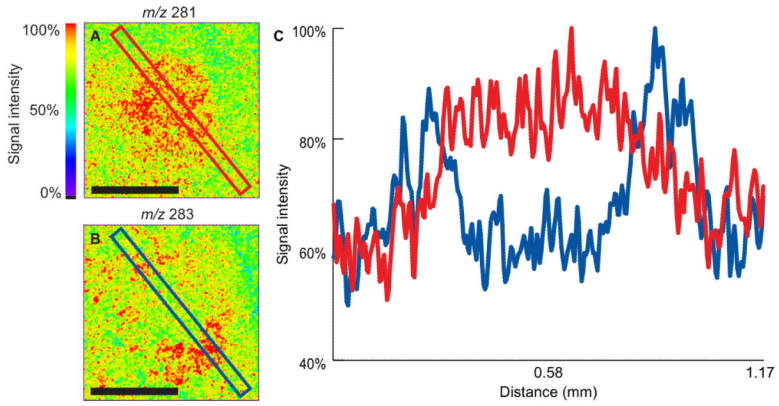

Figure 4.

Linescan analysis of LMAN. ToF-SIMS images showing the distribution of **(A)** oleic acid (*m/z* 281, 18:1 n-9) and (B) stearic acid (*m/z* 283, 18:0). (C) Linescan shows the relative intensity of the molecules across the images from the top left to the bottom right. Scale bar = 500 μm.

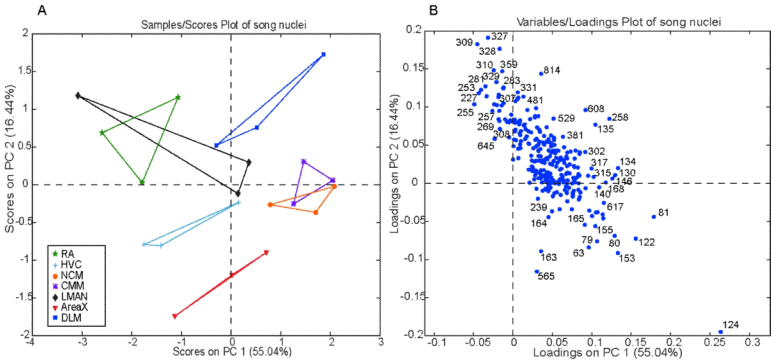

Figure 5.

Scores plot **(A)** from PCA using ToF-SIMS data collected from the different song nuclei. Each data point from a given song region represents data collected from a different adult brain. A line connects data representing the same song nuclei. Loadings plot **(B)** shows the masses responsible for the distribution of song nuclei in A.

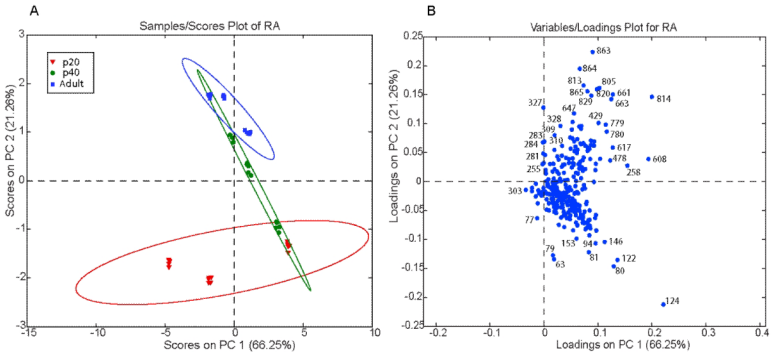

Figure 6.

Scores plot **(A)** from PCA using ToF-SIMS data collected from the RAs of post-hatch day 20, 40, and adult male zebra finches. Three different males from each age group were used, and five different spectra were collected from each RA. Ellipses are 95% confidence intervals. Loadings plot **(B)** shows the masses responsible for the distribution of the different aged RAs in A.

Table 1

Peak assignment for standards used in ToF-SIMS analysis using negative ion detection.

Molecule	Ion	Calculated	Measured	Designation
Phosphate	PO_2^-	63.0	63.0	Molecular ion
Phosphate	PO_3^-	79.0	79.0	Molecular ion
Phosphatidylethanolamine; PE	$C_2H_5NO_3P^-$	122.0	122.0	Head group
Phosphatidylethanolamine; PE	$C_2H_7NO_4P^-$	140.0	140.0	Head group
Myristic acid; 14:0	$C_{14}H_{27}O_2^-$	227.2	227.2	$[M-H]^-$
Palmitoleic acid; 16:1 n-7	$C_{16}H_{29}O_2^-$	253.2	253.2	$[M-H]^-$
Palmitic acid; 16:0	$C_{16}H_{33}O_2^-$	255.2	255.2	$[M-H]^-$
Linoleic acid; 18:2 n-6	$C_{18}H_{31}O_2^-$	279.2	279.2	$[M-H]^-$
Oleic acid; 18:1 n-9	$C_{18}H_{33}O_2^-$	281.2	281.2	$[M-H]^-$
Stearic acid; 18:0	$C_{18}H_{35}O_2^-$	283.3	283.3	$[M-H]^-$
Eicosapentaenoic acid; 20:5 n-3	$C_{20}H_{29}O_2^-$	301.2	301.2	$[M-H]^-$
Arachidonic acid; 20:4 n-6	$C_{20}H_{31}O_2^-$	303.2	303.2	$[M-H]^-$
8,11,14-Eicosatrienoic acid; 20:3 n-6	$C_{20}H_{33}O_2^-$	305.2	305.2	$[M-H]^-$
11,14-Eicosadienoic acid; 20:2 n-6	$C_{20}H_{35}O_2^-$	307.3	307.3	$[M-H]^-$
11-Eicosenoic acid; 20:1 n-9	$C_{20}H_{37}O_2^-$	309.3	309.3	$[M-H]^-$
Docosahexaenoic acid; 22:6 n-3	$C_{22}H_{31}O_2^-$	327.2	327.2	$[M-H]^-$
Adrenic acid; 22:4 n-6	$C_{22}H_{35}O_2^-$	331.3	331.3	$[M-H]^-$
Cholesterol	$C_{27}H_{43}O^-$	383.3	383.3	$[M-3H]^-$
Cholesterol	$C_{27}H_{45}O^-$	385.3	385.3	$[M-H]^-$
Cholesterol	$C_{27}H_{46}O^-$	386.3	386.3	$[M]^-$

Table 2

Average relative concentration of lipids across the different song nuclei. Relative concentrations are compared using a single factor ANOVA (n=3 birds), for the data within each row, i.e., the variation in signal among nuclei for a specific lipid. Data can also be compared within a single column for relative peak area for different lipids within a single brain area, but peak areas for different lipids are not necessarily proportional to their relative concentrations due to differences in ionization and detection.

Lipid	RA	LMAN	DLM	HVC	NCM	CMM	AreaX
Myristic acid; 14:0	1.2	1.7	1.2	1.8	1.0	1.4	1.0
Palmitoleic acid; 16:1 n-7**	2.9	3.5	2.6	3.1	2.4	2.7	2.6
Palmitic acid; 16:0	39.3	31.4	29.9	33.4	27.6	29.0	33.2
Linoleic acid; 18:2 n-6	2.2	3.0	2.9	2.7	2.1	2.5	2.5
Oleic acid; 18:1 n-9*	20.5	24.2	20.1	21.0	17.7	17.7	17.7
Stearic acid; 18:0**	19.7	17.9	27.3	21.8	23.4	23.9	21.6
Eicosapentaenoic acid; 20:5 n-3**	0.4	0.5	0.4	0.5	1.5	1.2	0.8
Arachidonic acid; 20:4 n-6***	2.4	3.1	2.5	3.1	9.3	6.2	4.9
8,11,14-Eicosatrienoic acid; 20:3n-6*	0.9	1.6	1.1	1.2	1.5	1.5	1.4
11,14-Eicosenoic acid; 20:2 n-6	0.9	1.0	0.9	1.0	0.8	1.0	0.8
11-Eicosenoic acid; 20:1 n-9*	1.0	1.2	1.4	1.1	0.7	0.8	0.8
Docosahexaenoic acid; 22:6 n-3	1.1	1.7	1.5	0.9	1.1	1.1	1.4
Adrenic acid; 22:4 n-6*	0.6	1.3	0.9	0.8	1.0	0.9	0.9
Cholesterol	6.7	8.0	7.4	7.5	10.0	10.2	10.5

* denotes p-value < 0.05

** p-value < 0.01

*** p-value < 0.0001.